

Article

¹³C-NMR Study on Structure Evolution Characteristics of High-Organic-Sulfur Coals from Typical Chinese Areas

Qiang Wei  and **Yuegang Tang** *

College of Geoscience and Surveying Engineering, China University of Mining and Technology, Beijing 100083, China; 13811880740@126.com

* Correspondence: tyg@cumtb.edu.cn; Tel.: +86-10-6233-9302

Received: 8 January 2018; Accepted: 30 January 2018; Published: 1 February 2018

Abstract: The structure evolution characteristics of high-organic-sulfur (HOS) coals with a wide range of ranks from typical Chinese areas were investigated using ¹³C-CP/MAS NMR. The results indicate that the structure parameters that are relevant to coal rank include CH₃ carbon (f_{al^*}), quaternary carbon, CH/CH₂ carbon + quaternary carbon (f_{al^H}), aliphatic carbon (f_{al^C}), protonated aromatic carbon (f_a^H), protonated aromatic carbon + aromatic bridgehead carbon (f_a^{H+B}), aromaticity (f_a^{CP}), and aromatic carbon (f_{ar^C}). The coal structure changed dramatically in the first two coalification jumps, especially the first one. A large number of aromatic structures condensed, and aliphatic structures rapidly developed at the initial stage of bituminous coal accompanied by remarkable decarboxylation. Compared to ordinary coals, the structure evolution characteristics of HOS coals manifest in three ways: First, the aromatic CH₃ carbon, alkylated aromatic carbon (f_a^S), aromatic bridgehead carbon (f_a^B), and phenolic ether (f_a^P) are barely relevant to rank, and abundant organic sulfur has an impact on the normal evolution process of coal. Second, the average aromatic cluster sizes of some super-high-organic-sulfur (SHOS) coals are not large, and the extensive development of cross bonds and/or bridged bonds form closer connections among the aromatic fringes. Moreover, sulfur-containing functional groups are probably significant components in these linkages. Third, a considerable portion of “oxygen-containing functional groups” in SHOS coals determined by ¹³C-NMR are actually sulfur-containing groups, which results in the anomaly that the oxygen-containing structures increase with coal rank.

Keywords: high-organic-sulfur coal; structure evolution; ¹³C-NMR

1. Introduction

Sulfur is one of the most hazardous elements in coal, and organic sulfur is more difficult to remove than other forms of sulfur in the conventional coal washing process. Thus, organic sulfur released during coal utilization could have severe adverse effect on the environment and human health. Generally, the coal with >1% organic sulfur is called high-organic-sulfur coal, and the organic sulfur content in super-high-organic-sulfur (SHOS) coal exceeds 4% [1,2]. The distribution of SHOS coals in the world is fairly limited. Croatia Raša coal is the representative with an incredible organic sulfur content of 11.4 wt % [3]. In addition, Spain Mequinenza lignite [4], New Zealand Charming Creek coal [5], India Tipong coal [6], and some coals from the Australia Gippsland Basin [7] are all SHOS coals. The SHOS coals in China are mainly part of the Late Permian coals in South China and primarily distributed in Guiding in Guizhou Province [8,9], Heshan in Guangxi Province [10,11], Chenxi in Hunan Province [12], Yanshan in Yunnan Province [13], Anxian in Sichuan Province [14], and Yishan in Guangxi Province [15]. Currently, it is controversial that the abundant “organic sulfur” in the SHOS coals is fully organically bound [16]. The existence of fine-grained pyrites

would be expected to increase the organic sulfur content determined by subtraction method [12]. Nevertheless, in the present study, these difference values are tentatively regarded as the contents of organic sulfur in coal. With regard to the formation of high organic sulfur and/or pyrite in coal, although seawater has been considered one of the major sources [2,17–19], hydrothermal fluid and special evolution mechanism could play critical roles. The multi-stage hydrothermal activity is one of the reasons for enrichment not only of pyrite [20,21] but also of organic sulfur [22], and the repeating reduction-reoxidation-disproportionation enrichment model proposed by Li and Tang [23] is another explanation for the abnormal enrichment of organic sulfur in coal. In addition, most sulfur in some SHOS coals (e.g., the Yanshan coal [13]) was likely influenced by submarine exhalation, which was carried into the peat swamp and then evenly distributed in the organic matter [13,16]. The hydrothermal fluids that have caused highly elevated S in coal are generally of epithermal origin [20] or are closely related to volcanic activities both in the marine (e.g., submarine exhalation) and in the terrestrial environments [24]. On the other hand, the SHOS coals in some cases contain highly-elevated critical elements that have a great potential for industrial extraction and utilization (e.g., rare earth elements, Y, V, Se, Mo, U) [3,25,26].

The nondestructive solid-state ^{13}C -NMR technique has been widely used during the last four decades [27–39] due to its potential for coal characterization. The wide application of ^{13}C cross polarization magic angle spinning (CP/MAS) technique has significantly promoted our knowledge on coal chemical structures [40–48]. Spectral-editing and peak-fitting techniques have been well established to identify specific functional groups from the spectra [49–52], and the high-resolution NMR methods allow for the measurement of the relative abundance of aromatic, aliphatic, phenolic, and carboxylic carbons [53,54]. Moreover, the chemical structures of coal lithotypes and macerals were also investigated by ^{13}C -NMR [55,56]. This technique has developed into an indispensable analytical method for coal macromolecular characterization [57–60].

There have been extensive studies on coal structure, organic sulfur structure in coal, and the structure evolution characteristics of ordinary coals. However, systematic studies on the structure of HOS coals are still limited, and the structure evolution characteristics of HOS coals are rarely reported. Besides, several S-containing coal structure models (Figure 1; [61–64]) have been proposed previously for a better understanding of coal structure, but the impact of abundant organic sulfur on coal structure remains unclear. The present study aims to investigate the compositional variations of aromatic carbons, aliphatic carbons, and oxygen-containing functional groups versus coal rank of HOS coals from typical Chinese areas; in addition, we explored the influence of abundant organic sulfur on the coal structure evolution. It could provide us new perspectives on the relationship between high organic sulfur and coal structure, and be potentially helpful for removing organic sulfur in the HOS coals.

Coal structure is one of the major characteristics of the coal rank that is formed in different conditions including geological setting, type of peat-forming plants, paleoclimate, and paleo-hydrological regime [48]. Besides, pressure and temperature play significant roles in modifying the deposition environment and the chemical structure of deposited biopolymers, which leads to the formation of coals with various ranks [65–68]; whereas the length of the formation time is an additional factor determining coal quality [69]. Therefore, it is not surprising that structure differences exist between coals sharing the same rank, and the structure characteristics of certain coals do not correspond to the overall evolution trend.

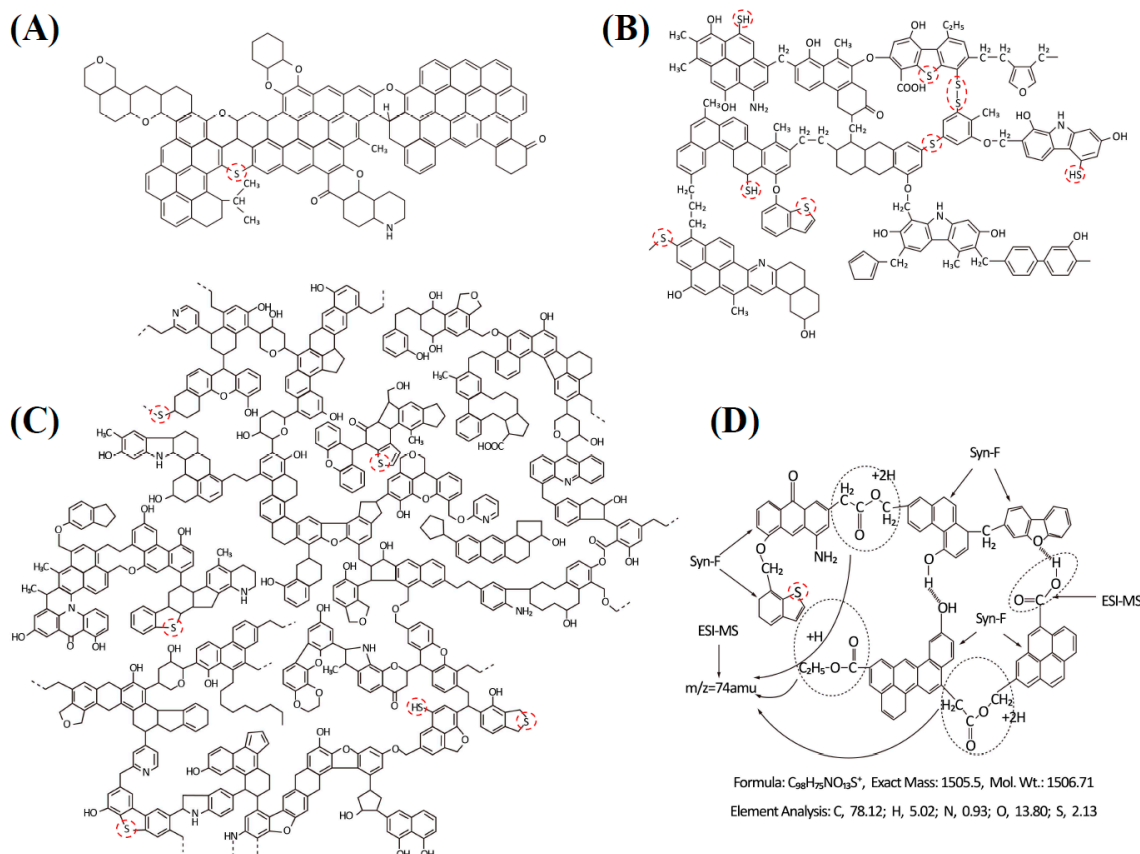


Figure 1. Typical S-containing coal structure models. (A) Fuchs' model [61]; (B) Wiser's model [62]; (C) Shinn's model [63]; (D) Ye's model; Syn-F, synchronous fluorescence spectroscopy; ESI-MS, electrospray ionization mass spectrometry; amu, atomic mass unit [64].

2. Samples and Analytical Methods

Nine HOS bench samples across a wide range of coal ranks were collected from different locations in China (Figure 2 and Table 1). The span of their maximum vitrinite/huminite reflectances (from 0.293% to 3.934%; Table 1) covers four coalification jumps (i.e., R_{max} around 0.6%, 1.3%, 2.5%, and 3.7%, respectively). The samples from southern China (JJP, CM, 6K, and GH) are all of a Late Permian age; while most of the samples from northern China (WHS, XY, SSP, and WTP) are Late Carboniferous coals, and the only lignite sample YX was collected from a Middle Jurassic coal seam. Each sample was stored in plastic bags to avoid from contamination and oxidation, and all samples were air dried before subsequent analyses.

The maximum reflectance determination was conducted using ASTM Standard D2798-05 [70], and the maceral classification applied in the present study was based on ICCP System 1994 [71, 72]. Proximate and ultimate analyses were performed using ASTM Standards D3173-03, D3175-02, D3174-04, and D3176-15 [73–76]. The total sulfur and forms of sulfur were determined following ASTM Standards D3177-02 and D2492-02 [77,78], respectively.

¹³C-NMR analyses were performed using a Bruker AVANCE III-400 MHz spectrometer with the CP/TOSS (cross polarization/ total suppression of spinning sidebands) pulse program (5.8 μs) at the Peking University Analytical Instrumentation Center, Beijing, China. A ¹³C resonance frequency of 100 MHz and a static magnetic field of 9.37 T were used for the experiments. The samples were ground to pass through a 200-mesh sieve and packed into a cylindrical zirconia rotor that was 4 mm in diameter. Cross polarization (contact time 3000 μs) with magic angle spinning (MAS) was applied at 5 KHz. 5200 scans were required to obtain the ¹³C spectra using a double-resonance probe head,

and the acquisition time and sweep width were 0.05 s and 300 ppm, respectively. Topspin 3.0 was used as the testing software.



Figure 2. Sampling locations of high-organic-sulfur coals in the present study.

Table 1. Basic information about vitrinite/huminite reflectance, sampling location, and geological background of high-organic-sulfur coals.

Sample	Seam-Bench	R _{max} ¹ (%)	Location	Mine	Age	Formation	Area
YX	1-1 ²	0.293	Dayou, Gansu	Yongxing Mine	Middle Jurassic	Yaojie Formation	Northern China
JJP	8-5	0.724	Chenxi, Hunan	Jiangjiaping Mine	Late Permian	Wujiaping Formation	Southern China
WHS	9-17	1.078	Wuda, Inner Mongolia	Wuhushan Mine	Late Carboniferous	Taiyuan Formation	Northern China
XY	10-3	1.150	Fenxi, Shanxi	Xinyu Mine	Late Carboniferous	Taiyuan Formation	Northern China
CM	6-1	1.404	Guiding, Guizhou	Caimiao Mine	Late Permian	Changxing Formation	Southern China
SSP	11-5	1.752	Hancheng, Shaanxi	Sangshuping Mine	Late Carboniferous	Taiyuan Formation	Northern China
6K	3-9	1.801	Heshan, Guangxi	Heshan No.6 Mine	Late Permian	Heshan Formation	Southern China
GH	M9-1	1.804	Yanshan, Yunnan	Ganhe Mine	Late Permian	Wujiaping Formation	Southern China
WTP	15-4	3.934	Jincheng, Shanxi	Wangtaipu Mine	Late Carboniferous	Taiyuan Formation	Northern China

R_{max}, maximum vitrinite/huminite reflectance, oil immersion. ¹ Two decimals are usually required for vitrinite/huminite reflectance values, but three decimals are used in the present study to distinguish close values for SHOS coal samples 6K and GH (1.801% and 1.804%, respectively). ² The Yongxing Mine has only one coal seam.

The chemical shifts and assignment for the ¹³C-NMR spectra of coal and its precursor have been summarized in previous studies [57–60,79–85], and the reported chemical shifts are mostly identical with only minor differences. The ¹³C-NMR structure parameters and assignment used in the present study are given in Table 2 [84,86–88]. Prior to deconvolution, the ¹³C-NMR spectrum was adjusted

using the Nuts Software. Then, the PFM module of the Origin Software was used to subtract the baseline, add peaks manually according to the spectrum shape and assignment of NMR structure parameters, and adjust the position, height, and full width at half maximum for every peak to make the fitted curve as close as possible to the test spectrum.

Table 2. Structure parameters and assignment for the ^{13}C -NMR spectra of coal [84,86–88].

Parameter	Assignment	Chemical Shift (ppm)
f_{al}^*	CH_3 carbon ¹	0–25
f_{al}^{H}	CH/CH_2 carbon + quaternary carbon ²	25–51
f_{al}^{O}	aliphatic carbon bonded to oxygen ³	51–90
$f_a^{\text{H}+\text{B}}$	protonated aromatic carbon + aromatic bridgehead carbon	90–137
f_a^{H}	protonated aromatic carbon	90–129
f_a^{N}	non-protonated aromatic carbon	129–165
$f_a^{\text{B}+\text{S}}$	aromatic carbon bonded to carbon	129–150
f_a^{B}	aromatic bridgehead carbon	129–137
f_a^{S}	alkylated aromatic carbon	137–150
f_a^{P}	phenolic ethers	150–165
f_a^{C}	carbonyl/carboxyl carbon ⁴	165–220
f_a^{CP}	aromaticity	90–165
f_a^{C}	aliphatic carbon	0–90
f_{al}^{C}	aromatic carbon	90–220
X_{BP}	ratio of aromatic bridgehead carbon to aromaticity	(129–137)/(90–165)

¹ Aliphatic CH_3 carbon (0–16 ppm), aromatic CH_3 carbon (16–25 ppm). ² CH/CH_2 carbon (25–36 ppm), quaternary carbon (36–51 ppm). ³ Methoxyl/aromatic methoxyl (51–75 ppm), aliphatic carbon bonded to oxygen in cyclic hydrocarbon (75–90 ppm). ⁴ Carboxyl carbon (165–188 ppm), carbonyl carbon (188–220 ppm).

3. Results

3.1. Basic Petrographic and Chemical Data

Basic data, including maceral composition, proximate analysis, ultimate analysis, and total sulfur and forms of sulfur of the HOS coals are shown in Table 3. The organic sulfur content of Sample WTP (0.95%, Table 3) is a bit below 1%, which is, as mentioned above, taken as the criterion of least organic sulfur content for HOS coals, but this sample is also included in the present study due to its high rank. All samples are dominated by vitrinite/huminite macerals (65.0–96.6%), and inertinite components (0.5–32.7%) come next. The liptinite macerals cannot be observed in most samples, except for Samples YX, WHS, and GH that contain 2.0–2.9% liptinites.

Table 3. Maceral composition, proximate analysis, ultimate analysis, and total sulfur and forms of sulfur in high-organic-sulfur coals.

Sample	Maceral ¹ (%)			Proximate Analysis (%)			Ultimate Analysis (%)			Total Sulfur and Forms of Sulfur (%)					
	V/H	I	L	M _{ad}	A _d	V _{daf}	C _{daf}	H _{daf}	N _{daf}	O _{daf}	S _{t,d}	S _{p,d}	S _{s,d}	S _{o,d}	S _{o,d} /S _{t,d}
YX	96.6	0.5	2.9	17.51	12.38	44.84	72.83	4.79	1.08	19.00	4.07	2.01	0.04	2.02	50
JJP	72.5	27.5	0.0	0.19	5.28	39.00	80.61	5.41	0.65	3.26	10.08	0.53	0.00	9.55	95
WHS	79.3	18.7	2.0	0.36	5.16	24.02	nd	nd	nd	2.48	0.06	0.01	2.41	97	
XY	77.7	22.3	0.0	0.70	2.58	21.71	88.01	4.73	1.24	2.89	3.26	0.22	0.00	3.04	93
CM	94.0	6.0	0.0	0.42	15.65	21.06	82.98	4.83	0.49	1.45	9.27	0.60	0.02	8.65	93
SSP	84.0	16.0	0.0	0.40	18.71	17.14	84.21	4.04	1.07	4.53	5.53	0.48	0.05	5.00	90
6K	77.5	22.5	0.0	0.32	23.62	14.27	82.34	3.46	0.58	1.03	10.44	0.80	0.02	9.62	92
GH	65.0	32.7	2.3	0.44	15.08	12.53	80.67	3.10	0.67	2.23	12.09	0.77	0.00	11.32	94
WTP	86.1	13.9	0.0	4.00	9.33	5.84	94.34	2.53	0.78	1.30	1.06	0.11	0.00	0.95	89

V, vitrinite; H, huminite; I, inertinite; L, liptinite; M, moisture; A, ash yield; V, volatile matter; C, carbon; H, hydrogen; N, nitrogen; O, oxygen; S_t, total sulfur; S_p, pyritic sulfur; S_s, sulfate sulfur; S_o, organic sulfur, by difference; ad, air-dry basis; d, dry basis; daf, dry and ash-free basis; nd, no data. ¹ Mineral free basis.

The volatile-matter yield, carbon content, hydrogen content, and H/C ratio display clear correlations with maximum reflectance of HOS coals (Figure 3A–D), suggesting that they could

be regarded as indicating parameters for coal rank. As expected for lignite, Sample YX has much higher oxygen content than other samples, and the oxygen content generally shows a decreasing trend versus coal rank (Figure 3E). It seems that the nitrogen content has nothing to do with the coal rank due to its variable trend (Figure 3F).

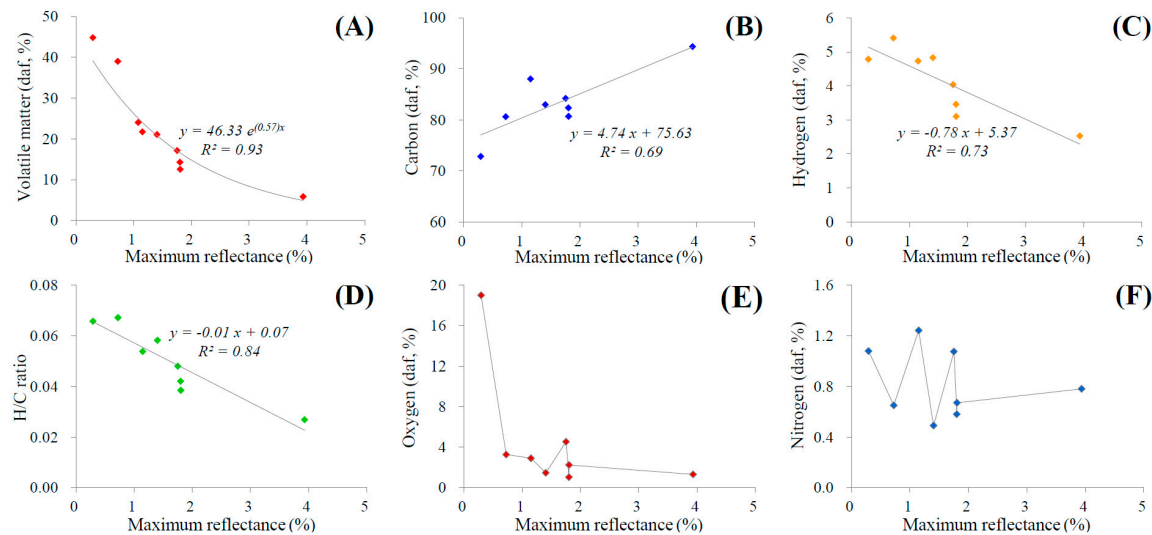


Figure 3. Relationships between selected proximate/ultimate parameters and maximum reflectance of vitrinite/huminite (R_{\max}) of high-organic-sulfur (HOS) coals. (A) volatile matter vs. R_{\max} ; (B) carbon content vs. R_{\max} ; (C) hydrogen content vs. R_{\max} ; (D) hydrogen/carbon ratio vs. R_{\max} ; (E) oxygen content vs. R_{\max} ; (F) nitrogen content vs. R_{\max} .

Generally, sulfide mineral (e.g., pyrite that contains pyritic sulfur) is one of the causes for coal combustion residual; thus, there should be a positive correlation between pyritic sulfur and ash yield. Meanwhile, pyritic sulfur and organic sulfur are usually negatively correlated to each other, especially when sulfate sulfur is negligible. Therefore, a negative correlation should exist between ash yield and organic sulfur. However, in the present study, the variation of ash yield across HOS coals (except for Samples YX and SSP) is generally compatible to that of organic sulfur content (Figure 4A). A possible explanation to this observation is that the organic sulfur contents derived from subtraction method are not definitively accurate, because a portion of sulfur occurring in fine-grained S-containing minerals that are dispersed in organic matter as inclusions were mistaken as organically associated, especially for the SHOS coals, as suggested by Li et al. [12]. The negative correlations between oxygen/nitrogen and organic sulfur (Figure 4B,C) indicate a limited capacity of coal macromolecular structure for heteroatoms. Part of bonding sites that can be assigned to oxygen and nitrogen are taken up by organic sulfur in the HOS coals.

3.2. ^{13}C -NMR Spectra and Peak-Fitting Results of HOS Coals

The solid-state ^{13}C -CP/MS NMR spectra of the HOS coals are shown in Figure 5. From the qualitative perspective, each spectrum exhibits two broad bands that represent aliphatic carbons (<90 ppm) and aromatic carbons (>90 ppm), respectively. With increasing coal rank, aliphatic carbons decrease gradually and aromatic carbons increase along with the aromatic bands becoming more thin and sharp, indicating an increasing maturity of the coal. Besides, the spectrum of aromatic carbons becomes smoother as coal rank grows, suggesting an increasing homogeneity of chemical structure. The satisfactory peak-fitting effect (Figure 6) is the prerequisite for reliable deconvolution results. Based on the ^{13}C -NMR structure assignment, each spectrum can be resolved into as many as twelve bands (Table 4).

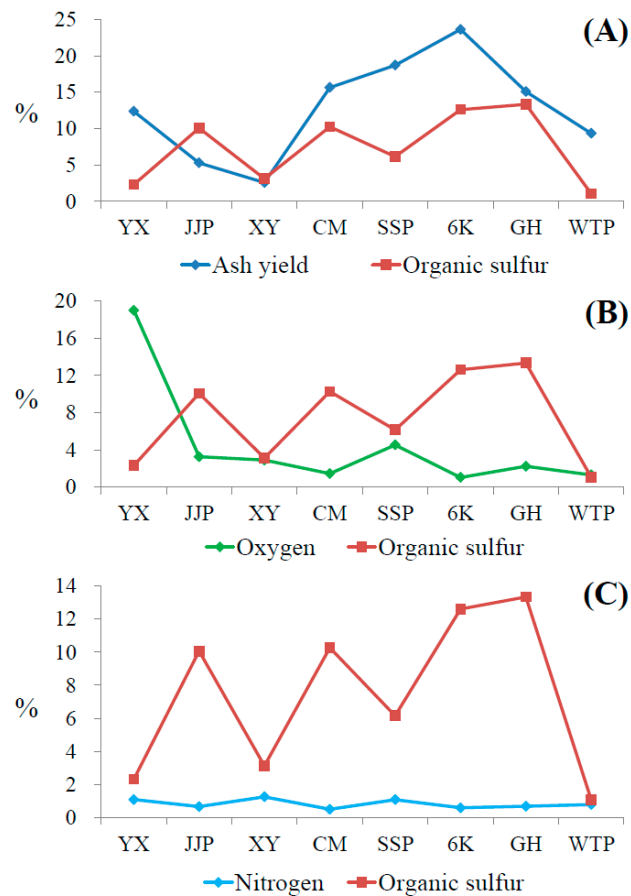


Figure 4. Relationships between selected proximate/ultimate parameters and organic sulfur content ($S_{o,d}$) of HOS coals. (A) ash yield vs. $S_{o,d}$; (B) oxygen content vs. $S_{o,d}$; (C) nitrogen content vs. $S_{o,d}$.

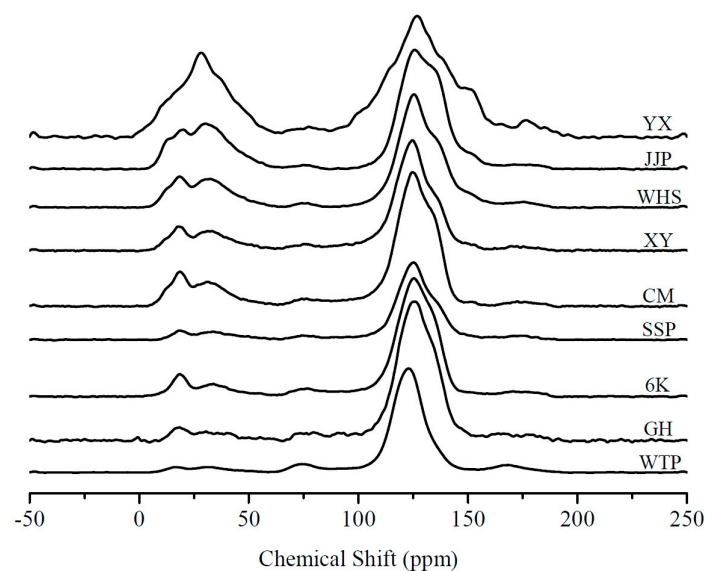


Figure 5. Solid-state ^{13}C -NMR spectra of high organic sulfur coals with increasing rank from top to bottom.

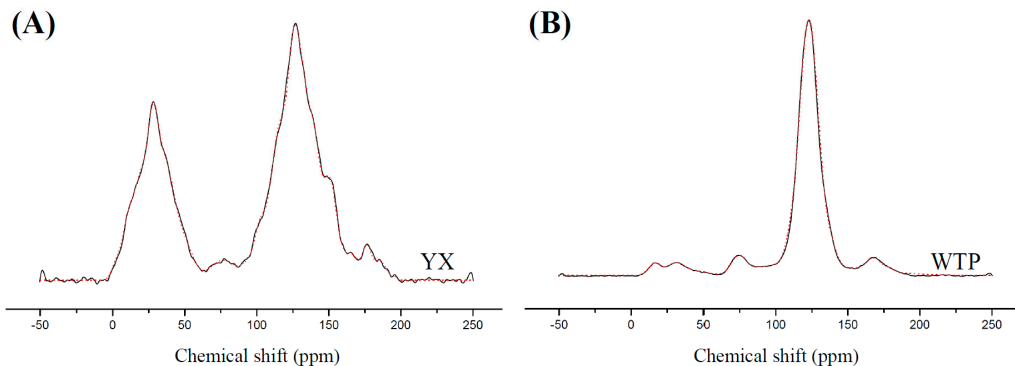


Figure 6. Peak-fitting effect for ^{13}C -NMR spectra. The test spectra are solid black, and the curve-fitted lines are dotted red. (A) Sample YX; (B) Sample WTP.

Table 4. ^{13}C -NMR peak-fitting results of high-organic-sulfur coals (%).

Sample	f_{al}^*				f_{al}^{H}				f_{al}^{O}	f_{al}^{C}	f_{a}^{H}
	0–16	16–25	20–25	25–36	36–51	25–51	51–75	75–90	51–90	0–90	90–129
YX	5.49	5.18	10.67	7.68	15.92	23.60	-	2.96	2.96	37.23	31.48
JJP	4.33	1.32	5.64	20.28	5.63	25.92	-	0.90	0.90	32.46	40.88
WHS	3.90	2.67	6.57	15.24	3.35	18.59	-	1.32	1.32	26.47	47.04
XY	2.83	3.36	6.19	9.81	4.31	14.11	1.42	-	1.42	21.73	61.97
CM	4.05	3.31	7.36	11.59	1.42	13.00	0.88	3.72	4.60	24.97	62.51
SSP	-	3.48	3.48	6.75	1.05	7.81	-	1.30	1.30	12.59	66.92
6K	1.42	4.05	5.48	7.30	-	7.30	1.40	3.87	5.28	18.05	60.99
GH	-	3.52	3.52	2.63	1.99	4.62	2.01	2.02	4.04	12.18	55.70
WTP	-	2.08	2.08	3.20	0.90	4.10	3.45	-	3.45	9.63	74.15
Sample	f_{a}^{B}	f_{a}^{S}	$f_{\text{a}}^{\text{B+S}}$	f_{a}^{P}	f_{a}^{N}	f_{a}^{CP}		f_{a}^{C}	f_{ar}^{C}	X_{BP}	
	129–137	137–150	129–150	150–165	129–165	90–165	165–188	188–220	165–220	90–220	(129–137)/(90–165)
YX	7.89	9.93	17.82	8.01	25.83	57.31	5.42	0.05	5.46	62.77	0.14
JJP	19.27	3.18	22.45	2.55	25.01	65.89	1.65	-	1.65	67.54	0.29
WHS	17.47	3.94	21.41	2.87	24.29	71.33	2.20	-	2.20	73.53	0.24
XY	11.51	1.64	13.15	0.90	14.04	76.01	2.26	-	2.26	78.27	0.15
CM	8.99	0.37	9.37	0.86	10.23	72.74	2.29	-	2.29	75.03	0.12
SSP	12.99	1.84	14.83	3.54	18.36	85.29	2.12	-	2.12	87.41	0.15
6K	9.96	3.91	13.88	5.27	19.15	80.14	1.82	-	1.82	81.95	0.12
GH	22.54	4.69	27.24	0.19	27.42	83.12	4.70	-	4.70	87.82	0.27
WTP	8.67	2.93	11.59	2.02	13.61	87.76	2.61	-	2.61	90.37	0.10

The unit for chemical shift is ppm.

4. Discussion

Carbon content and oxygen/carbon ratio were chosen as parameters of coal rank by Zhang [89] to explore the carbon structure evolution characteristics of low-to-medium rank coals using ^{13}C -NMR. Zhang's results demonstrated that there is a good correlation between aromatic carbon (f_{ar}^{C}), protonated aromatic carbon (f_{a}^{H}), aromatic bridgehead carbon (f_{a}^{B}), phenolic ethers (f_{a}^{P}), alkylated aromatic carbon (f_{a}^{S}), aliphatic carbon (f_{al}^{C}), aromatic CH₃ carbon, and aliphatic CH₃ carbon vs. coal rank. In the present study, maximum reflectance of vitrinite/huminite (R_{max}) was selected as the coal rank parameter, and the variations in the ^{13}C -NMR structure parameters versus R_{max} are shown in Figure 7. Aliphatic CH₃ carbon, CH₃ carbon (f_{al}^*), quaternary carbon, CH/CH₂ carbon + quaternary carbon (f_{al}^{H}), aliphatic carbon (f_{al}^{C}), protonated aromatic carbon (f_{a}^{H}), protonated aromatic carbon + aromatic bridgehead carbon ($f_{\text{a}}^{\text{H+B}}$), aromaticity (f_{a}^{CP}), and aromatic carbon (f_{ar}^{C}) exhibit clear relevance with coal rank. Thus, in comparison with ordinary coals, the structure evolution of the HOS coals does not display an apparent relationship between aromatic CH₃ carbon, aromatic bridgehead carbon (f_{a}^{B}), phenolic ethers (f_{a}^{P}), and alkylated aromatic carbon (f_{a}^{S}) vs. coal rank, suggesting that abundant organic sulfur has an impact on coal structure evolution.

^{13}C -NMR structure parameters can be divided into three categories as follows: aliphatic carbons, aromatic carbons, and oxygen-containing functional groups.

4.1. Aliphatic Carbon Evolution Characteristics of HOS Coals

4.1.1. Aliphatic Carbon (f_{al}^C)

A negative correlation is shown between aliphatic carbon and coal rank (Figure 7J). The variation trend at low-to-medium rank is relatively steep, and it becomes a gentle slope as the rank increases. The maximum at approximately R_{max} 1.404% (Sample CM) could be related to the second coalification jump, and another maximum exists around R_{max} 1.801% (Sample 6K).

4.1.2. CH_3 Carbon (f_{al}^*)

0–25 ppm is the combined effect scope of aliphatic CH_3 carbons (0–16 ppm) and aromatic CH_3 carbons (16–25 ppm). The aliphatic CH_3 carbons decrease significantly from low to medium rank (R_{max} 0.293–1.80%) and are completely detached at higher rank (Figure 7A). This indicates that the chain structures progressively break off during the coalification process.

The proportion of aromatic CH_3 carbons in lignite (Sample YX) is the largest, and it decreases in anthracite (Sample WTP). It is important to note that the aromatic CH_3 carbons increase with coal rank in the whole bituminous stage (Figure 7B). This variation indicates that there is no shortage of aromatic structures in lignite, and they are highly dispersed. Sufficient aromatic bonding sites lead to high aromatic methyl content. The coal structure suffered immense alteration in the first coalification jump, and the aromatic structures condensed at the initial stage of bituminous coal resulting in a decrease in the quantity of bonding sites for aromatic methyl. The increasing content of aromatic methyl in the bituminous coal stage is due to the extension of aromatic structures. As for anthracite, the aromatic structures experienced severe polycondensation, which resulted in the decrease of aromatic CH_3 carbons.

The combination of aliphatic CH_3 carbons and aromatic CH_3 carbons brought a generally negative correlation between CH_3 carbons (f_{al}^*) and coal rank (Figure 7C). Specifically, the increase in aromatic CH_3 carbons is more pronounced in the first half of the bituminous stage, and the decrease in aliphatic CH_3 carbons is dominant in the second half of the bituminous stage.

4.1.3. CH_2/CH Carbon + Quaternary Carbon (f_{al}^H)

The content of methylene and methyne represents the development degree of the chain structures in coal, and the average length of the aliphatic chains (Table 5) can be calculated through the ratio of the sum of methylene and aliphatic methyl to aliphatic methyl [90]. Overall, the average length gradually shortens except for lignite (Sample YX). The large quantity of CH_3 carbons (f_{al}^*) and low content of CH_2/CH carbons in lignite (Figure 7C,D) suggest that the aliphatic chains in Sample YX are widespread, but they are generally short and undeveloped. The chain structures experienced a large expansion at the beginning of bituminous coal stage; afterwards, the chain structures gradually shortened. When R_{max} reached 1.752% (Sample SSP), the aliphatic chains vanished due to the absence of aliphatic methyl. As an exception, the average length of aliphatic chains in Sample 6K is the longest among all studied samples and is not in line with the general variation trend (Table 5), which warrants further study.

Table 5. Average length of aliphatic chains in high-organic-sulfur coals.

Sample	YX	JJP	WHS	XY	CM	SSP	6K	GH	WTP
Length of aliphatic chains	2.40	5.69	4.91	4.46	3.86	-	6.13	-	-

Unit length is the average C–C bond length in aliphatic chains.

In addition, quaternary carbons decrease substantially with coal rank (Figure 7E). At the initial stage of bituminous coal, the increase in CH_2/CH carbons is more severe than the decrease in quaternary carbons, which results in a small rise in f_{al}^H followed by a dramatic decrease (Figure 7D–F).

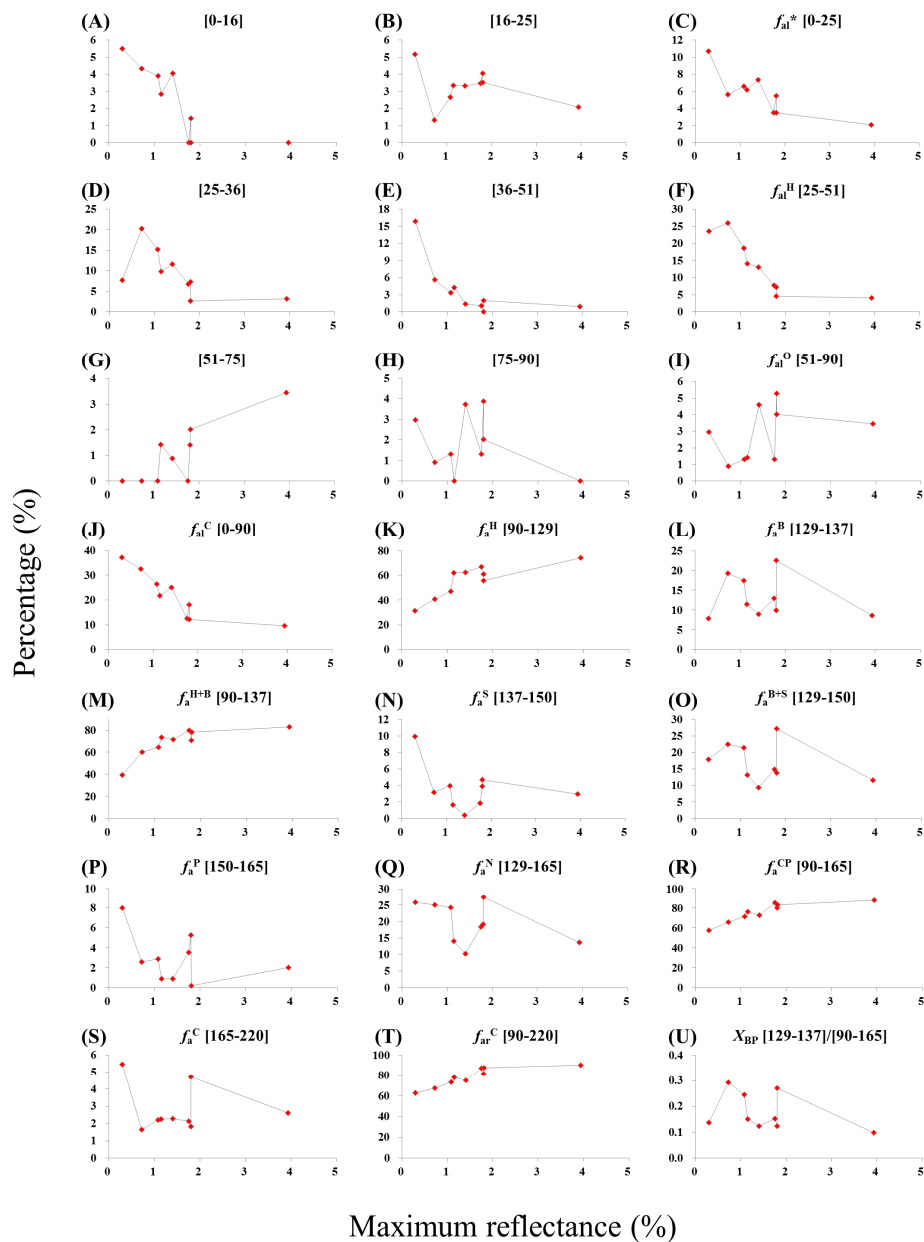


Figure 7. Variations of ^{13}C -NMR structure parameters versus maximum vitrinite/huminite reflectance (R_{\max} , %). The unit for chemical shift is ppm. (A) aliphatic CH_3 carbon [0–16] vs. R_{\max} ; (B) aromatic CH_3 carbon [16–25] vs. R_{\max} ; (C) CH_3 carbon (f_{al}^*) [0–25] vs. R_{\max} ; (D) CH/ CH_2 carbon [25–36] vs. R_{\max} ; (E) quaternary carbon [36–51] vs. R_{\max} ; (F) CH/ CH_2 carbon + quaternary carbon (f_{al}^{H}) [25–51] vs. R_{\max} ; (G) methoxyl/aromatic methoxyl [51–75] vs. R_{\max} ; (H) aliphatic carbon bonded to oxygen in cyclic hydrocarbon [75–90] vs. R_{\max} ; (I) aliphatic carbon bonded to oxygen (f_{al}^{O}) [51–90] vs. R_{\max} ; (J) aliphatic carbon (f_{al}^{C}) [0–90] vs. R_{\max} ; (K) protonated aromatic carbon (f_a^{H}) [90–129] vs. R_{\max} ; (L) aromatic bridgehead carbon (f_a^{B}) [129–137] vs. R_{\max} ; (M) protonated aromatic carbon + aromatic bridgehead carbon ($f_a^{\text{H+B}}$) [90–137] vs. R_{\max} ; (N) alkylated aromatic carbon (f_a^{S}) [137–150] vs. R_{\max} ; (O) aromatic carbon bonded to carbon ($f_a^{\text{B+S}}$) [129–150] vs. R_{\max} ; (P) phenolic ethers (f_a^{P}) [150–165] vs. R_{\max} ; (Q) non-protonated aromatic carbon (f_a^{N}) [129–165] vs. R_{\max} ; (R) aromaticity (f_a^{CP}) [90–165] vs. R_{\max} ; (S) carbonyl/carboxyl carbon (f_a^{C}) [165–220] vs. R_{\max} ; (T) aromatic carbon (f_{ar}^{C}) [90–220] vs. R_{\max} ; (U) ratio of aromatic bridgehead carbon to aromaticity (X_{BP}) [129–137]/[90–165] vs. R_{\max} .

4.2. Aromatic Carbon Evolution Characteristics of HOS Coals

Three main parameters are widely used for coal aromaticity characterization as follows: aromatic carbon (f_{ar}^C), aromaticity (f_a^{CP}), and the ratio of aromatic bridgehead carbon to aromaticity (X_{BP}).

4.2.1. Aromatic Carbon (f_{ar}^C) and Aromaticity (f_a^{CP})

Aromatic carbons exhibit a positive correlation with R_{max} (Figure 7T); thus, it can be regarded as an alternative parameter for coal rank determination. The aromatic carbon content is slightly lower than expected at R_{max} 1.404% (Sample CM) due to its low inertinite content (6.0%; Table 3), which bears a higher degree of condensation relative to vitrinite/huminite. The aromaticity also displays a positive correlation versus R_{max} (Figure 7R), and its steady variation suggests a gradual quantity growth of aromatic fringes during the coalification process.

4.2.2. Ratio of Aromatic Bridgehead Carbon to Aromaticity (X_{BP})

The parameter X_{BP} refers to the percentage of aromatic bridgehead carbons in all aromatic carbons, which characterizes the average aromatic cluster size of the coal macromolecule; in general, the value of this parameter increases with coal rank. Aromatization predominates in the low-to-medium metamorphic stage of coal, in other words, the aliphatic chains break off to form aromatic rings; while, condensation is dominant in the medium-to-high metamorphic stage, which means that the simple aromatic rings are condensed into polynuclear structures.

In the present study, the significant variation trend of X_{BP} is dependent on that of aromatic bridgehead carbon due to the gradual change of aromaticity across all samples (Figure 7L,R,U). The gradual variations in f_{ar}^C and f_a^{CP} indicate that coals with similar ranks possess equivalent amounts of aromatic carbons and aromatic fringes; accordingly, they should have comparable average sizes for aromatic clusters. Therefore, in theory, X_{BP} should also display a gradual variation trend, which is incompatible with the observation made in this study (Figure 7U). Since aromatic fringes are not the causes for this contradiction, it is likely due to the structures between aromatic fringes. The most reasonable explanation for this anomaly is that the high X_{BP} values of Samples JJP, WHS, and GH are abnormal, and their aromatic clusters are not that large; however, the extensive development of cross bonds and/or bridged bonds results in closer connections between aromatic fringes. Besides, the Samples JJP and GH are typical SHOS coals, and sulfur-containing functional groups are likely to be significant components in these linkages.

In addition, both protonated aromatic carbon (f_a^H) and aromatic bridgehead carbon (f_a^B) show variable trends across all HOS coals (Figure 7K,L), but the sum of them (f_a^{H+B}) exhibits a gradual trend and a positive correlation versus coal rank (Figure 7M). Non-protonated aromatic carbon (f_a^N) and aromatic carbon bonded to carbon (f_a^{B+S}) share similar variation trends (Figure 7O,Q).

4.3. Oxygen-Containing Functional Group Evolution Characteristics of HOS Coals

Carbonyl/carboxyl carbon (f_a^C), phenolic ethers (f_a^P), and aliphatic carbon bonded to oxygen (f_{al}^O) are appropriate parameters for characterizing oxygen-containing functional groups in coal [91].

In the present study, the content variations of oxygen-containing functional groups vs. maximum reflectance of vitrinite/huminite are shown in Figure 8. As expected for lignite, Sample YX has the most oxygen-containing structures, which conforms to the characteristics of low-rank coals; specifically, phenolic ethers are the most abundant, and carbonyl/carboxyl carbon comes next and followed by aliphatic carbon bonded to oxygen. From lignite (Sample YX) to bituminous coal (Sample JJP), the significant drop of oxygen-containing structures demonstrates that they suffered from intense destruction during the first coalification jump. Coalification is typically a de-oxidation process; however, the variation of total oxygen-containing structures generally exhibits an increase with coal rank in the bituminous to anthracite stage. Among bituminous coals, the SHOS Samples CM, SSP, 6K, and GH are of abnormally high organic sulfur contents, and they have more

oxygen-containing structures than other HOS coals (except Sample JJP). Considering the similar chemical properties and atomic structures of sulfur and oxygen, the most likely explanation for this observation is that a considerable portion of the “oxygen-containing functional groups” determined by ^{13}C -NMR are actually sulfur-containing functional groups, which leads to the anomalous increase of oxygen-containing structures versus coal rank. This differs from the observations made in previous studies on the structure evolution characteristics of non-HOS coals. In addition, compared to other coals in the present study, the organic sulfur content of Sample WTP (anthracite) is relatively low, and its large proportion of oxygen-containing structures is possibly due to some functional groups being subjected to oxidation.

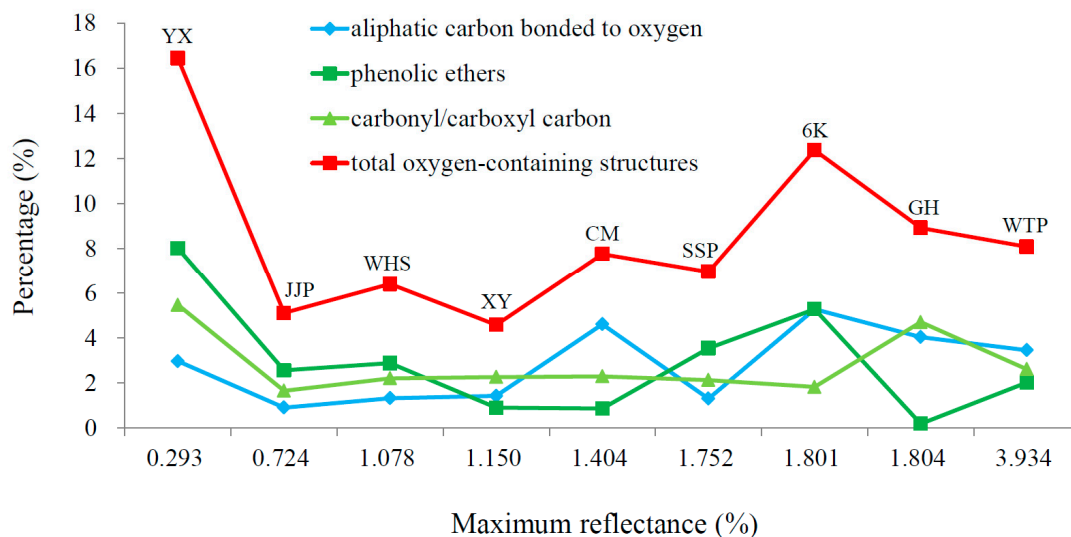


Figure 8. Variations in oxygen-containing functional groups versus coal rank of high organic sulfur coals.

4.3.1. Phenolic Ethers (f_a^P)

Besides the prominent maxima near the middle of the medium rank that correspond to Samples 6K and SSP, phenolic ethers exhibit a distinct decrease at low to medium rank (Figures 7P and 8), which results from continuous decomposition into CO_2 and H_2O .

4.3.2. Carbonyl/Carboxyl Carbon (f_a^C)

Generally, the content of carbonyl/carboxyl carbon decreases and decarboxylation persists in the whole coalification process. It reflects the characteristics of side chains falling off and aromaticity increasing. At first, the $-\text{OH}$ groups fall off during decarboxylation, and then, the proportion of $-\text{C}=\text{O}$ groups increases followed by the destruction of $-\text{C}=\text{O}$ groups [89].

Due to the negligible contents of carbonyl carbon (0–0.05%), the variation trend of f_a^C depends on that of the carboxyl carbon (Figure 7S and Table 4). Lignite has the highest content (5.42%) of carboxyl carbon, and the contents of all the bituminous coals are lower and comparable (1.65–2.29%) except Sample GH (4.70%) (Table 4), indicating the remarkable decarboxylation during the first coalification jump. The formation of thionocarboxylic groups is possibly responsible for the abnormally high carboxyl carbon content in Sample GH, which owns the most organic sulfur in the studied samples.

4.3.3. Aliphatic Carbon Bonded to Oxygen (f_{al}^O)

The proportion of methoxyl/aromatic methoxyl (51–75 ppm) increases generally with coal rank, with a dip at Sample SSP (R_{\max} 1.752%) (Figure 7G). By comparison, the variation in the aliphatic carbon bonded to oxygen in cyclic hydrocarbon (75–90 ppm) is much more complicated (Figure 7H). Thus,

the variation of f_{al}^O exhibits no correlation to coal rank (Figure 7I). In addition, Sample WTP (anthracite) has a low aliphatic/aromatic CH₃ carbon content and relatively high f_{al}^O content. In combination with the analysis of oxygen-containing structures above, the oxidized structures in Sample WTP can be inferred as methyls.

5. Conclusions

Each ¹³C-NMR spectrum of HOS coal can be resolved into as many as 12 peaks. The CH₃ carbon (f_{al}^*), quaternary carbon, CH/CH₂ carbon + quaternary carbon (f_{al}^H), aliphatic carbon (f_{al}^C), protonated aromatic carbon (f_a^H), protonated aromatic carbon + aromatic bridgehead carbon (f_a^{H+B}), aromaticity (f_a^{CP}), and aromatic carbon (f_{ar}^C) exhibit clear correlations with coal rank. Compared to ordinary coals, the structure evolution of HOS coals exhibits no correlations between the aromatic CH₃ carbon, aromatic bridgehead carbon (f_a^B), phenolic ethers (f_a^P), and alkylated aromatic carbon (f_a^S) versus rank, which suggests that high organic sulfur has an impact on the regular evolution process of coal structure.

The maximum of aliphatic carbon (f_{al}^C) at R_{max} 1.404% is due to the second coalification jump. There was no shortage of aromatic structures in lignite but were dispersed. The coal structure varied significantly in the first coalification jump, and the aromatic structures condensed at the initial stage of bituminous coal and stretched gradually in the whole bituminous stage. The aliphatic chains in lignite were widespread but generally short. These chains expanded greatly at the beginning of bituminous coal and then became shortened and detached before vanishing at around R_{max} 1.752%.

The aromatic fringes of HOS coals increase gradually in the coalification process, but the aromatic cluster size barely exhibits relevance to rank. It is inferred that the aromatic cluster sizes of some SHOS coals are not large, but the extensive development of cross bonds and/or bridged bonds form closer connections among aromatic fringes. In addition, sulfur-containing functional groups are likely to be significant components in these linkages.

For SHOS coals, a considerable portion of the “oxygen-containing functional groups” determined by ¹³C-NMR are actually sulfur-containing groups, which results in the anomaly that oxygen-containing structures increase versus coal rank. This indicates the substitution of oxygen by sulfur, which is also supported by the inverse correlation between oxygen and organic sulfur based on the ultimate analysis data. In addition, the decarboxylation is remarkable during the first coalification jump.

Acknowledgments: This research was supported by the National Key Basic Research Program of China (No. 2014CB238905) and the “111” Project (No. B17042). Hui Fu of the Analytical Instrumentation Center, Peking University is thanked for her help in performing the ¹³C-NMR analyses.

Author Contributions: Qiang Wei and Yuegang Tang conceived and designed the experiments and analyzed the data; Qiang Wei wrote the paper.

Conflicts of Interest: The authors declare no conflict of interest.

References

- Chou, C.-L. Geologic factors affecting the abundance, distribution, and speciation of sulfur in coals. In *Geology of Fossil Fuels, Proceedings of the 30th International Geological Congress: Part B, Beijing, China, 4–14 August 1996*; Yang, Q., Ed.; VSP: Utrecht, The Netherlands, 1997; Volume 18, pp. 47–57.
- Chou, C.-L. Sulfur in coals: A review of geochemistry and origins. *Int. J. Coal Geol.* **2012**, *100*, 1–13. [[CrossRef](#)]
- Sinninghe Damsté, J.S.; White, C.M.; Green, J.B.; de Leeuw, J.W. Organosulfur Compounds in Sulfur-Rich Raša Coal. *Energy Fuels* **1999**, *13*, 728–738. [[CrossRef](#)]
- White, C.M.; Collins, L.W.; Veloski, G.A.; Irdi, G.A.; Rothenberger, K.S.; Gray, R.J.; LaCount, R.B.; Kasrai, M.; Bancroft, G.M. A study of Mequinenza lignite. *Energy Fuels* **1994**, *8*, 155–171. [[CrossRef](#)]
- Torres-Ordonez, R.J.; Calkins, W.H.; Klein, M.T. Distribution of organic-sulfur-containing structures in high organic sulfur coals. In *Geochemistry of Sulfur in Fossil Fuels*; ACS Symposium Series; Orr, W.L., White, C.M., Eds.; American Chemical Society: Washington, DC, USA, 1990; pp. 287–295. ISBN 0841218048.

6. Calkins, W.H. The chemical forms of sulfur in coal: A review. *Fuel* **1994**, *73*, 475–484. [[CrossRef](#)]
7. Smith, J.W.; Batts, B.D. The distribution and isotopic composition of sulfur in coal. *Geochim. Cosmochim. Acta* **1974**, *38*, 121–133. [[CrossRef](#)]
8. Lei, J. Sulfur occurring regulation of Late Permian coal in Guizhou Province and component, structure and formation of high organosulfur coal. Ph.D. Thesis, China University of Mining and Technology, Beijing, China, 1993. (In Chinese with English Abstract).
9. Dai, S.; Seredin, V.V.; Ward, C.R.; Hower, J.C.; Xing, Y.; Zhang, W.; Song, W.; Wang, P. Enrichment of U–Se–Mo–Re–V in coals preserved within marine carbonate successions: Geochemical and mineralogical data from the Late Permian Guiding Coalfield, Guizhou, China. *Miner. Deposita* **2015**, *50*, 159–186. [[CrossRef](#)]
10. Shao, L.; Jones, T.; Gayer, R.; Dai, S.; Li, S.; Jiang, Y.; Zhang, P. Petrology and geochemistry of the high-sulphur coals from the Upper Permian carbonate coal measures in the Heshan Coalfield, southern China. *Int. J. Coal Geol.* **2003**, *55*, 1–26. [[CrossRef](#)]
11. Dai, S.; Zhang, W.; Seredin, V.V.; Ward, C.R.; Hower, J.C.; Song, W.; Wang, X.; Li, X.; Zhao, L.; Kang, H.; et al. Factors controlling geochemical and mineralogical compositions of coals preserved within marine carbonate successions: A case study from the Heshan Coalfield, southern China. *Int. J. Coal Geol.* **2013**, *109–110*, 77–100. [[CrossRef](#)]
12. Li, W.; Tang, Y.; Deng, X.; Yu, X.; Jiang, S. Geochemistry of the trace elements in the high-organic-sulfur coals from Chenxi coalfield. *J. China Coal Soc.* **2013**, *38*, 1227–1233, (In Chinese with English Abstract).
13. Dai, S.; Ren, D.; Zhou, Y.; Chou, C.-L.; Wang, X.; Zhao, L.; Zhu, X. Mineralogy and geochemistry of a super high-organic-sulfur coal, Yanshan Coalfield, Yunnan, China: Evidence for a volcanic ash component and influence by submarine exhalation. *Chem. Geol.* **2008**, *255*, 182–194. [[CrossRef](#)]
14. Ren, D.; Tang, Y.; Lei, J. Study on regularities of sulfur occurrence and pyrite magnetism of Late Permian coals in southwest China. *J. China Univ. Min. Technol.* **1994**, *4*, 64–73.
15. Dai, S.; Xie, P.; Ward, C.R.; Yan, X.; Guo, W.; French, D.; Graham, I.T. Anomalies of rare metals in Lopingian super-high-organic-sulfur coals from the Yishan Coalfield, Guangxi, China. *Ore Geol. Rev.* **2017**, *88*, 235–250. [[CrossRef](#)]
16. Dai, S.; Ren, D.; Zhou, Y.; Chou, C.L.; Wang, X.; Zhao, L.; Zhu, X. Multi-origin of synsedimentary volcanic ash and submarine exhalation for the enrichment of trace elements and minerals in coal. *Chin. Sci. Bull.* **2008**, *53*, 3120–3126, (In Chinese with English Abstract).
17. Lei, J.; Ren, D.; Tang, Y.; Chu, X.; Zhao, R. Sulfur-accumulating model of superhigh organosulfur coal from Guiding, China. *Chin. Sci. Bull.* **1994**, *39*, 1817–1821.
18. Dai, S.; Ren, D.; Tang, Y.; Shao, L.; Li, S. Distribution, isotopic variation and origin of sulfur in coals in the Wuda coalfield, Inner Mongolia, China. *Int. J. Coal Geol.* **2002**, *51*, 237–250. [[CrossRef](#)]
19. Dai, S.; Hou, X.; Ren, D.; Tang, Y. Surface analysis of pyrite in the No. 9 coal seam, Wuda Coalfield, Inner Mongolia, China, using high-resolution time-of-flight secondary ion mass-spectrometry. *Int. J. Coal Geol.* **2003**, *55*, 139–150. [[CrossRef](#)]
20. Dai, S.; Wang, X.; Seredin, V.V.; Hower, J.C.; Ward, C.R.; O’Keefe, J.M.K.; Huang, W.; Li, T.; Li, X.; Liu, H.; et al. Petrology, mineralogy, and geochemistry of the Ge-rich coal from the Wulantuga Ge ore deposit, Inner Mongolia, China: New data and genetic implications. *Int. J. Coal Geol.* **2012**, *90–91*, 72–99. [[CrossRef](#)]
21. Dai, S.; Yang, J.; Ward, C.R.; Hower, J.C.; Liu, H.; Garrison, T.M.; French, D.; O’Keefe, J.M.K. Geochemical and mineralogical evidence for a coal-hosted uranium deposit in the Yili Basin, Xinjiang, northwestern China. *Ore Geol. Rev.* **2015**, *70*, 1–30. [[CrossRef](#)]
22. Dai, S.; Zhang, W.; Ward, C.R.; Seredin, V.V.; Hower, J.C.; Li, X.; Song, W.; Wang, X.; Kang, H.; Zheng, L.; et al. Mineralogical and geochemical anomalies of late Permian coals from the Fusui Coalfield, Guangxi Province, southern China: Influences of terrigenous materials and hydrothermal fluids. *Int. J. Coal Geol.* **2013**, *105*, 60–84. [[CrossRef](#)]
23. Li, W.; Tang, Y. Sulfur isotopic composition of super high-organic-sulfur coals from the Chenxi coalfield, southern China. *Int. J. Coal Geol.* **2014**, *127*, 3–13. [[CrossRef](#)]
24. Dai, S.; Ward, C.R.; Graham, I.T.; French, D.; Hower, J.C.; Zhao, L.; Wang, X. Altered volcanic ashes in coal and coal-bearing sequences: A review of their nature and significance. *Earth-Sci. Rev.* **2017**, *175*, 44–74. [[CrossRef](#)]
25. Dai, S.; Yan, X.; Ward, C.R.; Hower, J.C.; Zhao, L.; Wang, X.; Zhao, L.; Ren, D.; Finkelman, R.B. Valuable elements in Chinese coals: A review. *Int. Geol. Rev.* **2016**. [[CrossRef](#)]

26. Dai, S.; Finkelman, R.B. Coal as a promising source of critical elements: Progress and future prospects. *Int. J. Coal Geol.* **2017**, in press. [[CrossRef](#)]
27. VanderHart, D.L.; Retcofsky, H.L. Estimation of coal aromaticities by proton decoupled carbon-13 magnetic resonance spectra of whole coals. *Fuel* **1976**, *55*, 202–204. [[CrossRef](#)]
28. Zilm, K.W.; Pugmire, R.J.; Larter, S.R.; Allan, J.; Grant, D.M. Carbon-13 CP/MAS spectroscopy of coal macerals. *Fuel* **1981**, *60*, 717–722. [[CrossRef](#)]
29. Wilson, M.A.; Pugmire, R.J.; Grant, D.M. Nuclear magnetic resonance spectroscopy of soils and related materials. Relaxation of ^{13}C nuclei in cross polarization nuclear magnetic resonance experiments. *Org. Geochem.* **1983**, *5*, 121–129. [[CrossRef](#)]
30. Newman, R.H.; Davenport, S.J. Comparison of Australasian tertiary coals based on resolution-enhanced solid-state ^{13}C n.m.r. spectra. *Fuel* **1986**, *65*, 533–540. [[CrossRef](#)]
31. Axelson, D.E. Solid state carbon-13 nuclear magnetic resonance study of Canadian coals. *Fuel Process. Technol.* **1987**, *16*, 257–278. [[CrossRef](#)]
32. Hatcher, P.G. Dipolar-dephasing ^{13}C -NMR studies of decomposed wood and coalified xylem tissue: Evidence for chemical structural changes associated with defunctionalization of lignin structural units during coalification. *Energy Fuels* **1988**, *2*, 48–58. [[CrossRef](#)]
33. Hatcher, P.G.; Lerch, H.E.; Verheyen, T.V. Organic geochemical studies of the transformation of gymnospermous xylem during peatification and coalification to subbituminous coal. *Int. J. Coal Geol.* **1989**, *13*, 65–97. [[CrossRef](#)]
34. Hatcher, P.G.; Wilson, M.A.; Vassallo, A.M.; Lerch, H.E. Studies of angiospermous wood in Australian brown coal by nuclear magnetic resonance and analytical pyrolysis: New insights into the early coalification process. *Int. J. Coal Geol.* **1989**, *13*, 99–126. [[CrossRef](#)]
35. Love, G.D.; Law, R.V.; Snape, C.E. Determination of nonprotonated aromatic carbon concentrations in coals by single pulse excitation carbon-13 NMR. *Energy Fuels* **1993**, *7*, 639–644. [[CrossRef](#)]
36. Maroto-Valer, M.M.; Taulbee, D.N.; Andresen, J.M.; Hower, J.C.; Snape, C.E. Quantitative ^{13}C -NMR study of structural variations within the vitrinite and inertinite maceral groups for semifusinite-rich bituminous coal. *Fuel* **1998**, *77*, 805–813. [[CrossRef](#)]
37. Freitas, J.C.C.; Bonagamba, T.J.; Emmerich, F.G. ^{13}C high resolution solid-state NMR study of peat carbonization. *Energy Fuels* **1999**, *13*, 53–59. [[CrossRef](#)]
38. Yoshida, T.; Sasaki, M.; Ikeda, K.; Mochizuki, M.; Nogami, Y.; Inokuchi, K. Prediction of coal liquefaction reactivity by solid state ^{13}C -NMR spectral data. *Fuel* **2002**, *81*, 1533–1539. [[CrossRef](#)]
39. Almendros, G.; Knicker, H.; Gonzalez-Vila, F.J. Rearrangement of carbon and nitrogen forms in peat after progressive thermal oxidation as determined by solid state ^{13}C - and ^{15}N -NMR spectroscopy. *Org. Geochem.* **2003**, *34*, 1559–1568. [[CrossRef](#)]
40. Crelling, J.C.; Schrader, R.H.; Benedict, L.G. Effects of weathered coal on coking properties and coke quality. *Fuel* **1979**, *58*, 542–546. [[CrossRef](#)]
41. Snape, C.E.; Axelson, D.E.; Botto, R.E.; Delpuech, J.J.; Tekely, P.; Gerstein, B.C.; Pruski, M.; Maciel, G.E.; Wilson, M.A. Quantitative reliability of aromaticity and related measurements on coals by ^{13}C n.m.r. A debate. *Fuel* **1989**, *68*, 547–560. [[CrossRef](#)]
42. Hatcher, P.G.; Faulon, J.L.; Wenzel, K.A.; Cody, G.D. A structural model for lignin-derived vitrinite from high-volatile bituminous coal (coalified wood). *Energy Fuels* **1992**, *6*, 813–820. [[CrossRef](#)]
43. Mukhopadhyay, P.K.; Hatcher, P.G. Composition of coal. In *Hydrocarbons from Coal*; Law, B.E., Rice, D.D., Eds.; AAPG: Tulsa, OK, USA, 1993; pp. 79–118. ISBN 0891810463.
44. Wilson, M.A.; Hanna, J.V.; Anderson, K.B.; Botto, R.E. ^1H CRAMPS NMR derived hydrogen distributions in various coal macerals. *Org. Geochem.* **1993**, *20*, 985–999. [[CrossRef](#)]
45. Botto, R.E. Fossil fuels. In *Encyclopedia of Nuclear Magnetic Resonance*; Grant, D.M., Harris, R.K., Eds.; John Wiley & Sons: New York, NY, USA, 1996; pp. 2101–2118. ISBN 978-0-471-95839-0.
46. Pugmire, R.J. Coal structure from solid state NMR. In *Encyclopedia of Nuclear Magnetic Resonance*; Grant, D.M., Harris, R.K., Eds.; Wiley: Chichester, UK, 1996; pp. 1355–1365. ISBN 0471958395.
47. Nanny, M.A.; Minear, R.A.; Leenheer, J.A. *Nuclear Magnetic Resonance in Environmental Chemistry*; Oxford University Press: New York, NY, USA, 1997; ISBN 0195097513.
48. Suggate, R.P.; Dickinson, W.W. Carbon NMR of coals: The effects of coal type and rank. *Int. J. Coal Geol.* **2004**, *57*, 1–22. [[CrossRef](#)]

49. Mao, J.; Cory, R.M.; McKnight, D.M.; Schmidt-Rohr, K. Characterization of a nitrogen-rich fulvic acid and its precursor algae from solid state NMR. *Org. Geochem.* **2007**, *38*, 1277–1292. [CrossRef]
50. Mao, J.; Tremblay, L.; Gagne, J.P.; Kohl, S.; Rice, J.; Schmidt-Rohr, K. Humic acids from particulate organic matter in the Saguenay Fjord and the St. Lawrence Estuary investigated by advanced solid-state NMR. *Geochim. Cosmochim. Acta* **2007**, *71*, 5483–5499. [CrossRef]
51. Mao, J.; Fang, X.; Lan, Y.; Schimmelmann, A.; Mastalerz, M.; Xu, L.; Schmidt-Rohr, K. Chemical and nanometer-scale structure of kerogen and its change during thermal maturation investigated by advanced solid-state ^{13}C -NMR spectroscopy. *Geochim. Cosmochim. Acta* **2010**, *74*, 2110–2127. [CrossRef]
52. Mao, J.; Palazzo, A.J.; Olk, D.C.; Clapp, C.E.; Senesi, N.; Bashore, T.L.; Cao, X. Chemical structure of soil organic matter in slickspots as investigated by advanced solid-state NMR. *Soil Sci.* **2010**, *175*, 329–338. [CrossRef]
53. Newman, R.H.; Sim, M.N.; Johnston, J.H.; Collen, J.D. Comparison of aromaticity and phenolic content as parameters for characterization of coal by ^{13}C n.m.r. spectroscopy. *Fuel* **1988**, *67*, 420–425. [CrossRef]
54. Dickinson, W.W.; Newman, R.H.; Price, L.C.; Sykes, R. ^{13}C -NMR Spectra and Selected Maturation Parameters from 15 Wells in Southern Taranaki Basin, New Zealand; Geology Board of Studies Publication No. 19; Research School of Earth Sciences, Victoria University of Wellington: Wellington, New Zealand, 1996; p. 31.
55. Liu, D.; Peng, P. Possible chemical structures and biological precursors of different vitrinites in coal measure in Northwest China. *Int. J. Coal Geol.* **2008**, *75*, 204–212. [CrossRef]
56. Cao, X.; Mastalerz, M.; Chappell, M.A.; Miller, L.F.; Li, Y.; Mao, J. Chemical structures of coal lithotypes before and after CO_2 adsorption as investigated by advanced solid-state ^{13}C nuclear magnetic resonance spectroscopy. *Int. J. Coal Geol.* **2011**, *88*, 67–74. [CrossRef]
57. Van Niekerk, D.; Pugmire, R.J.; Solum, M.S. Structural characterization of vitrinite-rich and inertinite-rich Permian-aged South African bituminous coals. *Int. J. Coal Geol.* **2008**, *76*, 290–300. [CrossRef]
58. Van Niekerk, D.; Mathews, J.P. Molecular representations of Permian-aged vitrinite-rich and inertinite-rich South African coals. *Fuel* **2010**, *89*, 73–82. [CrossRef]
59. Xiang, J.; Zeng, F.; Liang, H.; Sun, B.; Zhang, L.; Li, M.; Jia, J. Model construction of the macromolecular structure of Yanzhou Coal and its molecular simulation. *J. Fuel Chem. Technol.* **2011**, *39*, 481–488. [CrossRef]
60. Xiang, J.; Zeng, F.; Li, B.; Zhang, L.; Li, M.; Liang, H. Construction of macromolecular structural model of anthracite from Chengzhuang coal mine and its molecular simulation. *J. Fuel Chem. Technol.* **2013**, *41*, 391–399, (In Chinese with English Abstract). [CrossRef]
61. Fuchs, W.; Sandhoff, A.G. Theory of coal pyrolysis. *Ind. Eng. Chem.* **1942**, *34*, 567–571. [CrossRef]
62. Wiser, W.H. ACS Preprint, Division of Fuel Chemistry; American Chemical Society: Washington, DC, USA, 1975; p. 733.
63. Shinn, J.H. From coal to single stage and two-stage products: A reactive model of coal structure. *Fuel* **1984**, *63*, 1187–1196. [CrossRef]
64. Ye, C. Characterization and modeling of coal high molecular weight components. Ph.D. Thesis, Taiyuan University of Technology, Taiyuan, China, 2008. (In Chinese with English Abstract).
65. Wilson, M.A.; Verheyen, T.V.; Vassallo, A.M.; Hill, R.S.; Perry, G.J. Selective loss of carbohydrates from plant remains during coalification. *Org. Geochem.* **1987**, *11*, 265–271. [CrossRef]
66. Bates, A.L.; Hatcher, P.G. Solid-state ^{13}C -NMR studies of a large fossil gymnosperm from the Yallourn Open Cut, Latrobe Valley, Australia. *Org. Geochem.* **1989**, *14*, 609–617. [CrossRef]
67. Hatcher, P.G.; Clifford, D.J. The organic geochemistry of coal: From plant materials to coal. *Org. Geochem.* **1997**, *27*, 251–274. [CrossRef]
68. Crowell, D.L. Coal, an Educational Leaflet No. 8; Ohio Division of Natural Resources (ODNR). 2008; (revised). Available online: <http://geosurvey.ohiodnr.gov/portals/geosurvey/PDFs/Education/el08.pdf> (access on 31 January 2018).
69. Ussiri, D.A.N.; Jacinthe, P.; Lal, R. Methods for determination of coal carbon in reclaimed minesoils: A review. *Geoderma* **2014**, *214–215*, 155–167. [CrossRef]
70. ASTM International. *Test Method for Microscopical Determination of the Vitrinite Reflectance of Coal*; ASTM Standard, D2798-05; Gaseous Fuels, Coal and Coke; ASTM International: West Conshohocken, PA, USA, 2005.
71. International Committee for Coal and Organic Petrology (ICCP). The new vitrinite classification (ICCP System 1994). *Fuel* **1998**, *77*, 349–358.

72. International Committee for Coal and Organic Petrology (ICCP). The new inertinite classification (ICCP System 1994). *Fuel* **2001**, *80*, 459–471.
73. ASTM International. *Test Method for Moisture in the Analysis Sample of Coal and Coke*; ASTM Standard, D3173-03; Gaseous Fuels, Coal and Coke; ASTM International: West Conshohocken, PA, USA, 2005.
74. ASTM International. *Test Method for Volatile Matter in the Analysis Sample of Coal and Coke*; ASTM Standard, D3175-02; Gaseous Fuels, Coal and Coke; ASTM International: West Conshohocken, PA, USA, 2005.
75. ASTM International. *Test Method for Ash in the Analysis Sample of Coal and Coke from Coal*; ASTM Standard, D3174-04; Gaseous Fuels, Coal and Coke; ASTM International: West Conshohocken, PA, USA, 2005.
76. ASTM International. *Standard Practice for Ultimate Analysis of Coal and Coke*; ASTM Standard, D3176-15; Gaseous Fuels, Coal and Coke; ASTM International: West Conshohocken, PA, USA, 2015.
77. ASTM International. *Test Methods for Total Sulfur in the Analysis Sample of Coal and Coke*; ASTM Standard D3177-02; Gaseous Fuels, Coal and Coke; ASTM International: West Conshohocken, PA, USA, 2005.
78. ASTM International. *Standard Test Method for Forms of Sulfur in Coal*; ASTM Standard, D2492-02; Gaseous Fuels, Coal and Coke; ASTM International: West Conshohocken, PA, USA, 2005.
79. Yoshida, T.; Mackawa, Y. Characterization of coal structure by CP/MAS carbon-13 NMR spectrometry. *Fuel Process. Technol.* **1987**, *15*, 385–395. [[CrossRef](#)]
80. Xu, X.; Zhang, P. The study of carbon structure by solid-¹³C-NMR and XPS. *Coal Convers.* **1995**, *18*, 57–62, (In Chinese with English Abstract).
81. Kawashima, H.; Yamashita, Y.; Saito, I. Studies on structural changes of coal density-separated components during pyrolysis by means of solid-state ¹³C-NMR spectra. *J. Anal. Appl. Pyrolysis* **2000**, *53*, 35–50. [[CrossRef](#)]
82. Takanohashi, T.; Shishido, T.; Kawashima, H.; Saito, I. Characterisation of Hyper Coals from coals of various ranks. *Fuel* **2008**, *87*, 592–598. [[CrossRef](#)]
83. Wang, S.; Tang, Y.; Schobert, H.H.; Guo, Q.; Wang, F. Liquefaction reactivity and ¹³C-NMR of coals rich in barkinite and semifusinite. *J. Fuel Chem. Technol.* **2010**, *38*, 129–133, (In Chinese with English abstract). [[CrossRef](#)]
84. Li, Y.; Cao, X.; Zhu, D.; Chappell, M.A.; Miller, L.F.; Mao, J. Characterization of coals and their laboratory-prepared black carbon using advanced solid-state ¹³C nuclear magnetic resonance spectroscopy. *Fuel Process. Technol.* **2012**, *96*, 56–64. [[CrossRef](#)]
85. Wang, P.; Jin, L.; Liu, J.; Zhu, S.; Hu, H. Analysis of coal tar derived from pyrolysis at different atmospheres. *Fuel* **2013**, *104*, 14–21. [[CrossRef](#)]
86. Mei, Y.; Zhao, X.; Sun, W.; Tang, J.; Qiao, A. Spectral Analysis of Coal Tar from Xiaohuangshan Region. *Chin. J. Magn. Reson.* **2011**, *28*, 339–348, (In Chinese with English Abstract).
87. Mei, Y. Study on spectroscopy and performance potential of hydrocarbons in Xinjiang coal. Master's Thesis, Xinjiang University, Urumqi, China, 2011. (In Chinese with English Abstract).
88. Castro-Marcano, F.; Lobodin, V.V.; Rodgers, R.P.; McKenna, A.M.; Marshall, A.G.; Mathews, J.P. A molecular model for Illinois No. 6 Argonne Premium coal: Moving toward capturing the continuum structure. *Fuel* **2012**, *95*, 35–49. [[CrossRef](#)]
89. Zhang, Y. ¹³C-NMR research of coalification mechanism for low-medium rank coal. Master's Thesis, Taiyuan University of Technology, Taiyuan, China, 2006. (In Chinese with English Abstract).
90. Chen, D.; Hu, J.; Ye, C. The high resolution ¹³C-NMR study on Chinese coals. *Sci. China Ser. D* **1996**, *26*, 525–530, (In Chinese with English Abstract).
91. Luo, Y.; Li, W.; Chen, Y. ¹³C-NMR analysis on different macerals of several low-to-medium rank coals. *J. Fuel Chem. Technol.* **2005**, *33*, 540–543, (In Chinese with English Abstract).



© 2018 by the authors. Licensee MDPI, Basel, Switzerland. This article is an open access article distributed under the terms and conditions of the Creative Commons Attribution (CC BY) license (<http://creativecommons.org/licenses/by/4.0/>).